Full Length Article

Methyl passivation is better than silicon oxide passivation in five aspects for the Si/PEDOT:PSS interface

Yingfeng Li [*], Bingxin Wang, Mengqi Cui, Xiang Li, Meicheng Li [*]

State Key Laboratory of Alternate Electrical Power System with Renewable Energy Sources, North China Electric Power University, Beijing 102206, China

ABSTRACT

Methyl passivation has been demonstrated to be better than the silicon oxide passivation commonly used in Si/PEDOT:PSS solar cells; however, the reason is still unclear. Based on first-principle calculations on the carrier transport behaviors at the Si/PEDOT:PSS interface, we found that methyl passivation is superior to silicon oxide passivation in five aspects. First, methyl plays better than silicon oxide in eliminating the dangling bonds and introducing fewer defect levels in the bandgap. Secondly, the effective carrier mass in methyl passivated Si substrate is smaller than silicon oxide passivated. Thirdly, the carrier transfer rate through the Si/PEDOT:PSS interface with methyl passivation will be much larger than that with silicon oxide passivation. Fourthly, an additional electric field that can boost the separation of carriers will form at the methyl passivated Si/PEDOT:PSS interface. Finally, the energy band bending of the Si substrate with methyl passivation, ~0.08 eV, will not hinder the holes extraction as significantly as that with silicon oxide passivation, ~0.63 eV. This article provides a complete process for evaluating a passivation scheme based on first-principle calculations.

1. Introduction

Si/PEDOT:PSS hybrid solar cell has received extensive research in recent years, as it has the potential to become a substitute for crystalline Si solar cell [1]. The use of crystalline Si as the light absorber ensures the high power conversion efficiency (PCE) of the Si/PEDOT:PSS solar cell, which has reached 17% yet [2–7]. Meanwhile, the preparation cost of the Si/PEDOT:PSS solar cell is meager, as it only needs to spin or spray coat a PEDOT:PSS layer on the Si substrate under room temperature and normal pressure [8–11].

The critical factor restricting the PCE of the Si/PEDOT:PSS solar cell is that, at the organic/inorganic interface, many defects will bring severe recombination of the photo-generated carriers. Therefore, the sequentially refresh of the PCE records of Si/PEDOT:PSS solar cell is always accompanied by continual improvement of Interface passivations [4,12,13]. In 2011, the PCE record of the Si/PEDOT:PSS solar cell was 11%, where the interface is passivated by silicon oxide [14]; by 2014, a 13.5% PCE was achieved benefit from the methyl passivation [15]; till 2017, the PCE record reached 17.0%, where both surfaces of the silicon were passivated by siloxane oligomer [7].

Which passivation method is better can be reflected by experimental measurements of the minority carrier lifetime of the passivated Si substrate [16,17]. The minority carrier lifetime in methyl, siloxane oligomer, and silicon oxide passivated Si substrate is 35.8 μs, 35.0 μs, and 24.7 μs, respectively [7,18,19]. The longest minority carrier lifetime means that methyl passivation should be better than the other two passivation methods. Experimental measurement can even reflect whether the passivation layer promotes or hinders the extraction of carriers. For example, Kelvin force microscopy can give a cross-section electric potential curve through the interface [20]. Nevertheless, it is hard to reveal the carrier transmission behaviors at the electronic level based on experimental measurements.

First-principle calculations can explore the detailed electron structure-related properties. Based on first-principle calculations, Hong et al. have found that the dangling bonds on the Si surface severely hindered the doping efficiency [21]. Peelaers et al. have shown that the surface dangling bonds would trap electrons, thus reducing the conductivity [22]. Ko et al. have found that substitutional defects and surface dangling bonds reduced the conductance in silicon quantum wires [23]. However, no first-principle study evaluated the effects of various passivation methods for the Si/PEDOT: PSS interface has been reported.

In this work, we carried out first-principle calculations on the carrier transmission behaviors through the Si/PEDOT:PSS interface. The results revealed that five aspects of methyl passivation are better than silicon

---

oxide passivation: the fewer defect states, the smaller effective carrier mass, the stronger orbital coupling, the more favorable additional electric field, and the weaker energy band bending. Such insights are helpful for the choice of passivation technologies and provide a systematic evaluation method for them.

2. Model and computational details

2.1. Model

The proper Si/PEDOT:PSS interface model, which can authentically represent the actual system, is the precondition to ensure the significance of the simulations. Fig. 1 shows the construction process for the Si/PEDOT:PSS interface models.

2.1.1. Model of the silicon substrate

First, we tried to construct the bare Si(1 0 0) substrate. There exist four surface structures for Si (1 0 0) surface. According to the order of formation energy from small to large, they are the c(4 × 2), the p(2 × 2), the asymmetric p(2 × 1), and the symmetrical p(2 × 1) surfaces. The c(4 × 2) and p(2 × 2) ones are most commonly used in first-principle calculations. Smith, Roland, and Ji et al. have studied the adsorption behaviors of H_3Al, amino acetic acid, styrene, and $CH_3X(X = Br$ and Cl), on the c(4 × 2) Si(1 0 0) surface, respectively [24–28]. Jyh, Shing, and Lin et al. have investigated the reaction process between some organic molecules and the p(2 × 2) Si(1 0 0) surface [29–31]. As the p(2 × 2) Si (1 0 0) surface has a more diminutive size, we selected it as the Si substrate, as shown in Fig. 2.

A primary criterion for the rationality of the Si substrate in investigating the electron properties is that the density of state (DOS) of its intermediate layers can match that of a bulk Si. After comparison (*Supplementary Material S1*), we have found that the DOS diagram for the middle layers of Si substrate with eight layers is close to that of the bulk silicon. Therefore, the Si substrate was modeled to have 8-layers; and the top two layers were allowed to relax.

Next, we tried to construct the Si substrates with different passivation layers. Fig. 3a shows the methyl passivated Si substrate, where the topmost silicon atom bonds with a methyl group to saturate its suspension bond. For the silicon oxide passivated surface, we referred to the silica layer modeled by Pasquarello et al., [32,33] to model the silicon oxide layer. i.e., the tridymite P6/MMC-silica with a = b = 5.03 Å, c = 8.22 Å, α = β = 90°, and γ = 120°. The (−2 1 0) facet of silica was butt jointed with the Si(1 0 0) surface, which brought a mismatch of 7.0% and 13.4% along with the OA and OB directions, respectively, consistent with the reported results [34,35]. The Si (1 0 0) surface formed an "oxygen bridge" with the silica layer, as given in Fig. 3b.

2.1.2. Model of the PEDOT:PSS

PEDOT:PSS comprises positively-charged p-doped PEDOT (poly-3,4-ethylene dioxythiophene) and negatively-charged PSS (poly-4-styrene sulfonate). Several PEDOT: PSS models have been proposed, including the EDOT monomer (3, 4-ethylene dioxythiophene) [36], the tri-EDOT [37], the EDOT octamer, and the crystal model [38]. Of them, the crystal model is the only one that can provide the proper bandgap (1.6 ∼ 1.7 eV), band structure, and position of the highest occupied molecular orbital (HOMO) [39,40]. Therefore, we chose the rhombic crystal P2/c-PEDOT:PSS to model the PEDOT:PSS, as given in Fig. 4. A one-dimensional long chain represents the PEDOT along the OB direction, and the PSS is replaced by some discrete Tos (the monomer of the PSS chain). The PEDOT main chain is layered by π-π accumulation structure, and it presents sandwiched stacking structure with the Tos monomers.

Appropriately placing the PEDOT:PSS on Si substrate is crucial in constructing the Si/PEDOT:PSS model. At first, it has to determine which facet of the PEDOT:PSS crystal is more favorable for contacting the Si (1 0 0) substrate. For this reason, we established three Si/PEDOT: PSS interface models and carried out molecular dynamic calculations [41,42] to simulate the annealing process after the PEDOT:PSS has been spin-coated on the Si substrate (*Supplementary Material S2*) [43]. The binding energy E_{bind} between the PEDOT:PSS and the Si substrate was chosen as the criteria to determine which interface model is preferred. The E_{bind} for the Si/OAB-PEDOT:PSS model, as shown in Fig. 5a, is the lowest; therefore, the OAB facet of PEDOT:PSS crystal should contact the Si substrate.

However, the Si/OAB-PEDOT:PSS model in Fig. 5a has too many atoms for *DFT* calculation. Therefore, we took only one-quarter of it as the Si/OAB-PEDOT:PSS model used in the following calculations (Fig. 5b). In the simplified model, the PEDOT:PSS crystal in the OA direction took a quarter, while those in the OB and OC directions remained; the adjacent Tos groups' orientations were changed from opposite to the same; and the lattice parameter of the PEDOT:PSS crystal in the OB direction was compressed from 15.8 Å to 15.36 Å.

We have compared the DOS diagrams between the pristine and the simplified PEDOT:PSS (*Supplementary Material S3*). The results show that the simplification and compression will not significantly affect PEDOT:PSS's DOS, i.e., the simplified model can reasonably represent the actual electronic properties of PEDOT:PSS.

2.1.3. Model of the Si/PEDOT:PSS interface

The Si/PEDOT:PSS interface models were constructed based on the optimized Si substrate and the simplified PEDOT:PSS. Fig. 6 illustrates the optimized Si/ PEDOT:PSS models. A vacuum layer ∼ 15 Å was placed above the PEDOT:PSS to isolate its interaction with the bottom of the Si substrate.
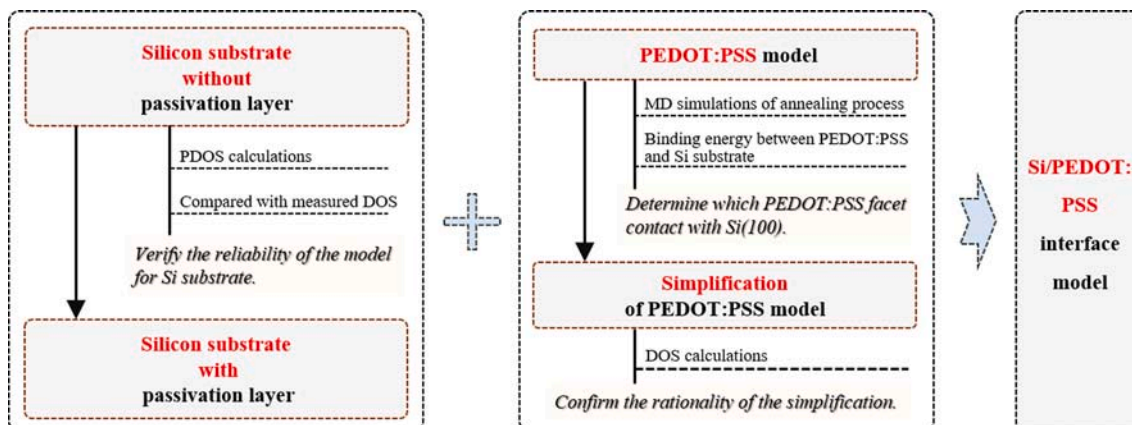

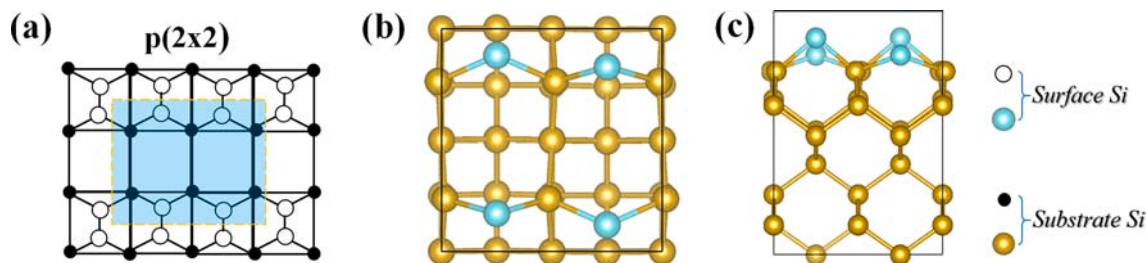**Fig. 1.** The construction process for the Si/PEDOT:PSS model.

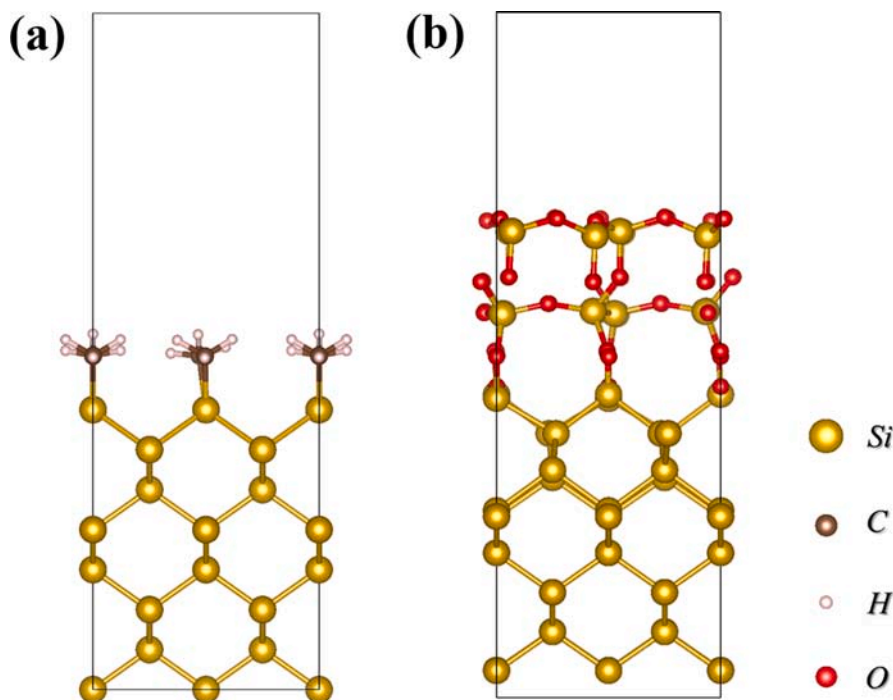**Fig. 2.** The top and side views of the p(2 × 2) reconstructed Si(1 0 0) surface.

Fig. 3. (a) methyl and (b) silicon oxide passivated Si substrates.

2.2. Computational details

The GGA-PBE functional previously used to calculate silicon's energy band structure and work function is selected [44]. The Norm-Conserving pseudo-potential is adopted, as it can give a DOS diagram of Si consistent with the experimental results [43,44]. The DFT-D grimme correction is added to describe the remote VDW interactions. The spin polarization correction is not included, as the DOS diagrams with and without spin polarization correction were almost overlapping for both bulk silicon and PEDOT:PSS crystal.

The cutoff energy is set to 830 eV; the k-point sampling is set as $2 \times 1 \times 1$. The convergence criteria of structure optimization are set as: the energy iteration difference less than 1×10^{-6} eV/atom, the maximum stress of an atom smaller than 0.02 eV/Å, and the SCF difference less than 0.5×10^{-6} eV/atom. The bottom two silicon layers are fixed in the optimization process, and the other layers are allowed to relax. In calculating the electronic properties, including the band structures, DOS diagram, charge density, and Mulliken distribution, the functional, pseudo-potential, and cutoff energy remain the same as those used in the optimization calculations, while a larger $4 \times 2 \times 1$ k-point grid is used for more accuracy. In the wave function analysis, only the Γ point is taken into account. We have chosen the quadratic difference method to calculate the effective mass of carriers. The isosurface value is set to 0.002 eV in the drawing of the wave function images.

We have carefully tested the reliability of the above calculation

settings by comparing the calculated results for the bulk silicon and the PEDOT:PSS crystal with the reported ones [18,38,45] (*Supplementary Material S4*).

3. Results and discussions

We have compared the impacts of methyl and silicon oxide passivations from six aspects: 1) chemical passivation for the defect states on the surface of Si substrate; 2) the effective carrier mass in the Si substrate; 3) the carrier transmission type through the interface, according to the overlap of wave functions at the conductive band-minimum (CBM) and the valence band-maximum (VBM); 4) the orbital coupling coefficient between Si-VBM and PEDOT:PSS-HOMO and between Si-CBM and PEDOT:PSS-HOMO, which can reflect the carrier transmission rate through the interface; and 5) the additional electric field through the interface based on Mulliken charge population analysis; and 6) the bands matching through the interface.

3.1. Chemical passivation for the surface defect states on Si substrate

Fig. 7 gives the DOS diagrams of the total interface system (TDOS), the sublayers of the Si substrate (PDOS-12, PDOS-45), and the passivation layers (PDOS-CH$_3$, PDOS-SiO$_x$). It can be observed from Fig. 7(a) that the forbidden band of the reconstructed bare Si substrate disappears but is filled by two prominent peaks, and from the PDOS, we can refer to
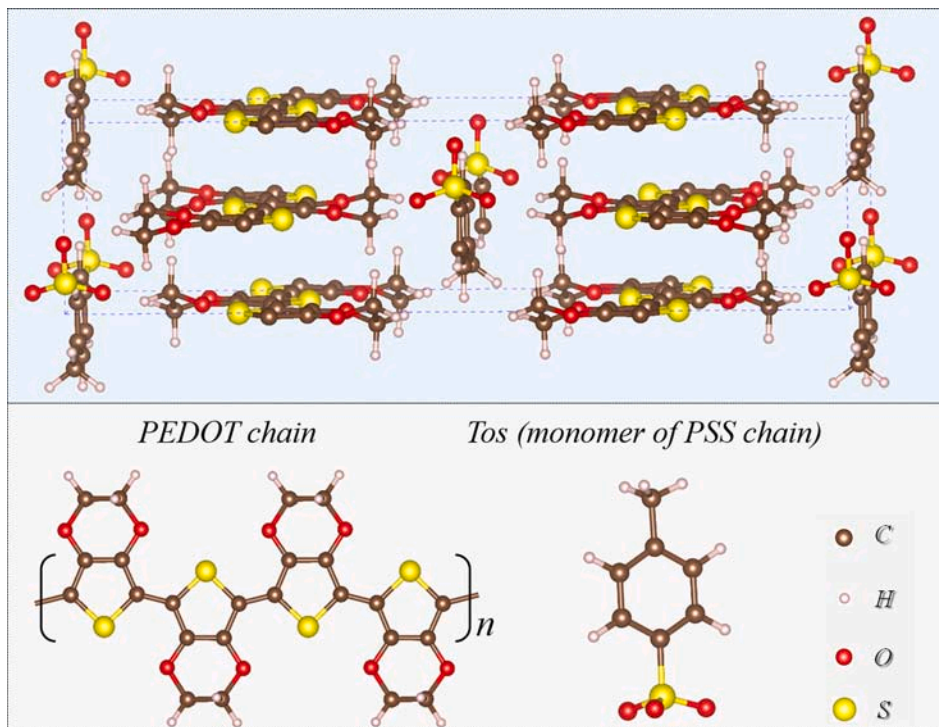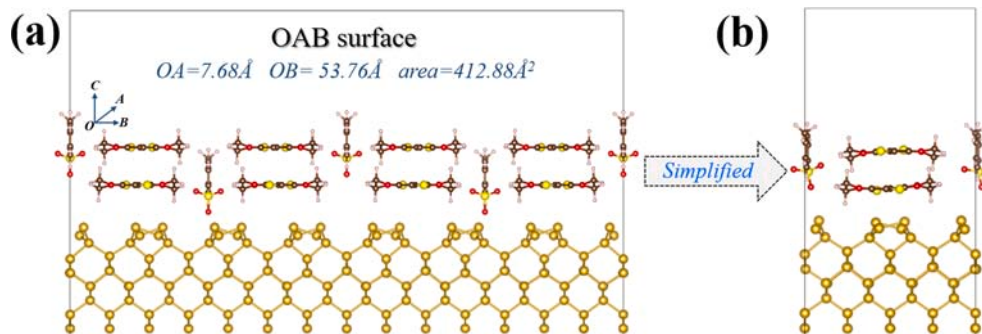
Fig. 4. Model of the PEDOT:PSS.

Fig. 5. The Si/PEDOT:PSS models. (a) the original model after molecular dynamic simulation; (b) the simplified one.

these two peaks to the 1st and 2nd Si atom layers. These phenomena mean that the reconstruction of the Si surface will bring many deep defect states.

However, from Fig. 7(b) we can see that the bandgap of the methyl passivated Si substrate is clean, and the PDOS curves of the Si atoms in the surface layer (1st, 2nd layers) and intermediate layer (4th, 5th layers) are almost entirely overlapping. The overlapping of the PDOS curves indicates that the dangling bonds on the 1st layer of the Si substrate are ideally eliminated, and the clean bandgap means that the methyl will not introduce additional defect states.

The passivation effect of silicon oxide is illustrated in Fig. 7(c). The weak peak in the bandgap near the top valence band denotes that there are still some defect states in the Si substrate. The PDOS curves show that the Si atoms in the 1st and 2nd layers contribute to these defect states. But other than that, the passivation effect of silicon oxide is similar to the case of methyl passivation. The PDOS of the 1st and 2nd layers generally overlaps with the 4th and 5th layers. Meanwhile, the silicon oxide layer hardly contributes to the DOS in the bandgap.

Besides, the bandgap of the methyl passivated Si substrate, ~0.7 eV, is closer to that of the bulk Si, 0.703 eV, than that of the silicon oxide passivate one, ~0.63 eV. Therefore, methyl almost doesn't affect the

bandgap of the Si substrate. The underestimation of bandgaps compared with the experimental value, 1.12 eV, should come from using the GGA-PBE functional.

In summary, both the methyl and the silicon oxide layer can provide effective chemical passivation for the Si surface. But comparatively speaking, methyl plays better than silicon oxide in eliminating the dangling bonds, introducing fewer defect levels in the bandgap, and bringing a more negligible impact on the Si substrate's band structure.

3.2. Effective carrier mass in the Si substrate

Effective carrier mass is an important basic parameter of a solid. In solid, the carrier moves in a periodic potential, and their movement can be very different from their motion in a vacuum. The effective carrier mass is a quantity used to simplify the impact of periodic potential by modeling the behavior of a free carrier with that mass. Therefore, a small effective carrier mass means that the carrier can move faster under the same driving force.

Passivation will induce extra stress on the Si substrate, affecting the periodic potential for the lateral movement of carriers and, therefore, the effective carrier mass. Table 1 gives the effective masses of electrons
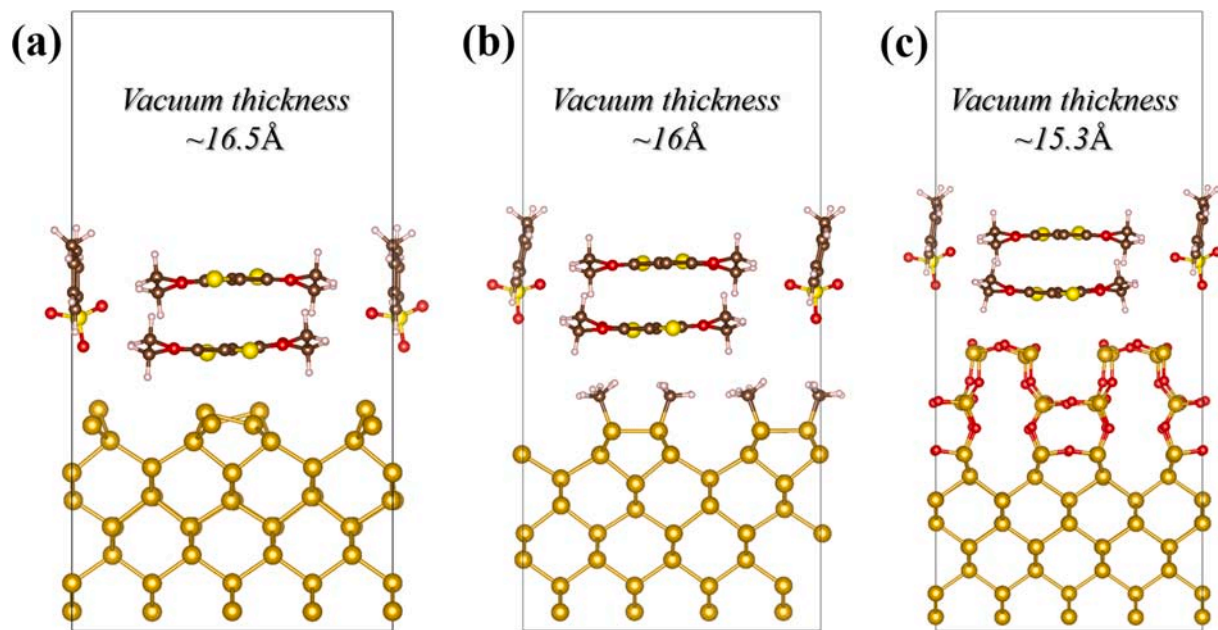
Fig. 6. The Si/OAB-PEDOT:PSS interface models with (a) bare, (b) methyl passivated, and (c) silicon oxide passivated Si substrate.
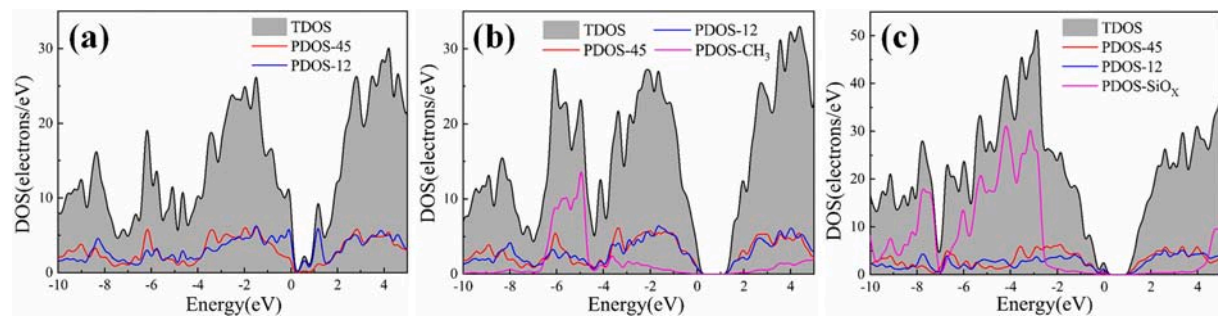

Fig. 7. DOS curves of the (a) reconstructed bare, (b) methyl passivated, and (c) silicon oxide passivated Si substrate. PDOS-12 and PDOS-45 denote the PDOS of layers $1 + 2$ and $4 + 5$ from top to bottom, respectively; PDOS-CH$_3$ and PDOS-SiO$_X$ denote the PDOS of the methyl and the silicon oxide layer.

Table 1
Effective carrier mass in Si substrate.

	The effective carrier mass (m_e)					
	Si (1 0 0)		Si (0 1 0)		Si (1 1 0)	
	Hole	Electron	Hole	Electron	Hole	Electron
Bare Si	−0.60	0.39	−15.59	1.54	−0.56	0.29
CH$_3$– Si	−0.34	0.36	−0.32	0.64	−0.32	0.36
SiO$_x$- Si	−0.32	0.64	−10.59	0.30	−0.28	0.20

and holes in the (1 0 0), (0 1 0), and (1 1 0) directions of the Si substrate. The effective carrier mass in the (0 0 1) direction cannot be obtained, as the energy band is discontinuous in this direction due to the vacuum layer.

We can see that the average effective electron masses in the methyl and silicon oxide passivated Si substrate, 0.45 m_e and 0.38 m_e, are smaller than that in the bare Si substrate, 0.74 m_e. The average effective hole mass in the methyl passivated Si substrate, 0.33 m_e, is much smaller than those in the silicon oxide passivated and bare Si substrate, 3.73 m_e and 5.58 m_e. Meanwhile, only in the methyl passivated Si substrate, the effective masses of electron and hole are almost the same in all three directions. The carrier mobility is inversely proportional to the square of the effective carrier mass. Therefore, the approximately equal effective masses of electron and hole mean that their mobilities are also roughly

equivalent, which is helpful for the solar cell's stable performance under high-intensity light irradiation. On the surface of silicon, sheet resistance becomes one of the primary resistances to charge migration. The approximately equal effective carrier masses in the lateral directions mean the difficulty of the carrier moving along the three directions is similar.

In conclusion, methyl passivation can reduce the effective carrier mass in the Si substrate more significantly than the silicon oxide passivation, thereby improving the interface carrier transmission rate. It should be mentioned that the reduction of carrier effective mass by passivation only works in the surface area of the Si substrate. However, as the model of Si substrate has only eight layers here, the effect seems to be more significant.

3.3. Carrier transmission type through the interface

The transmission type of electron and hole through the interface can be reflected by the overlap of wave functions at CBM and VBM, respectively. Fig. 8(a) gives the DOS diagram of the bare Si/PEDOT:PSS system, and Fig. 8(a.1) is its wave function image at the Fermi level. First, the wave function of the Si substrate and the PEDOT chain overlap significantly, which demonstrates that the holes transmission from the Si substrate to the PEDOT:PSS should be adiabatic. Then, the wave function is primarily distributed on the PEDOT layer closest to the Si substrate, which indicates that the holes may mainly transmit in the PEDOT
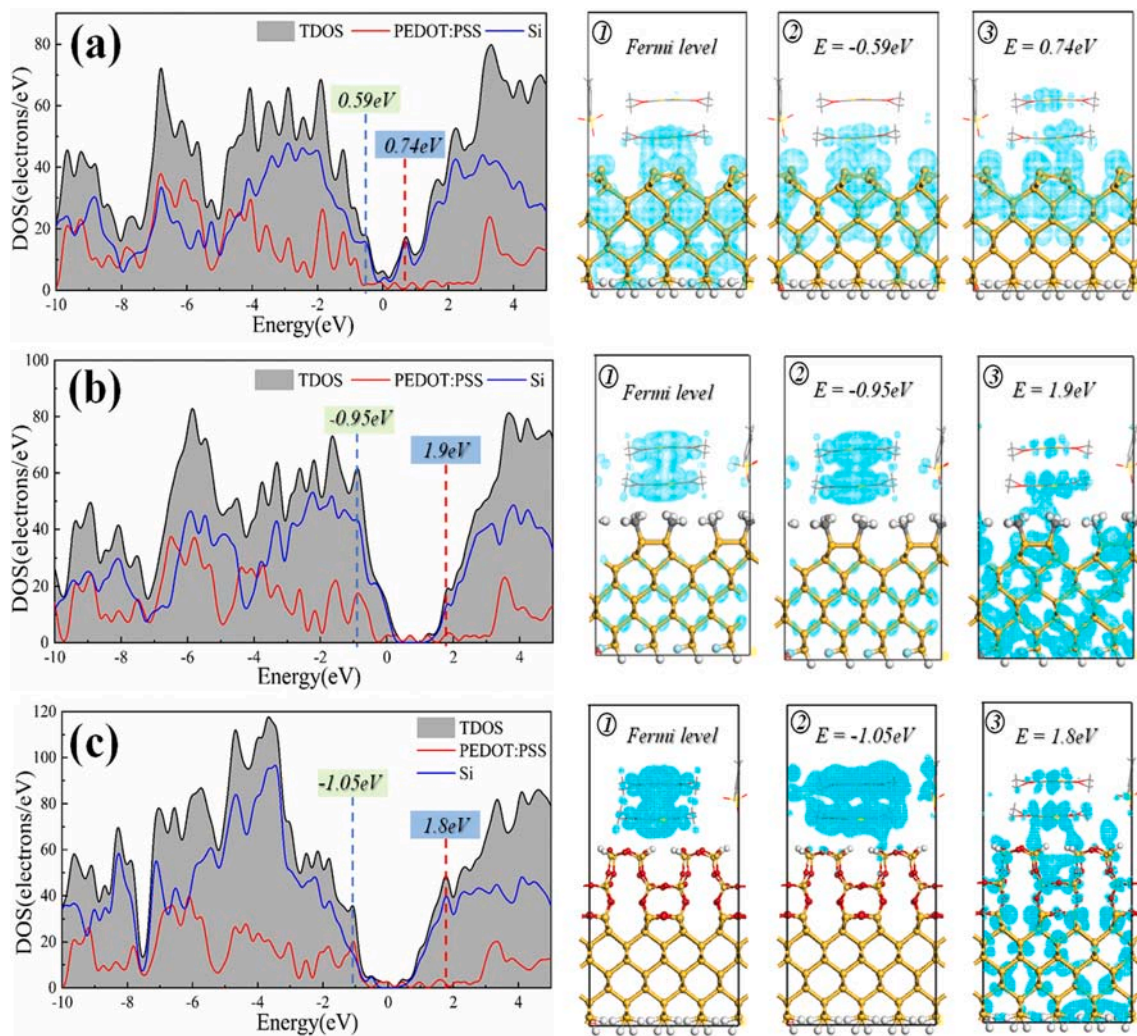
Fig. 8. DOS and wave function diagrams of the Si/PEDOT:PSS systems with (a) bare, (b) methyl passivated, and (c) silicon oxide passivated Si substrate. The wave function diagrams were labeled by numerals 1 to 3.

layer near the Si surface. This deduction is consistent with the fact that a higher efficiency Si/PEDOT:PSS solar cell usually has a thinner PEDOT: PSS layer. We have also drawn the wave function image on energy level $E = -0.59\ eV$ in Fig. 8(a.2). The shape and distribution are similar to those in Fig. 8(a.1), confirming the adiabatic intrinsic of hole transmission at the Si/PEDOT:PSS interface.

To analyze the electron transmission type through the Si/PEDOT:PSS interface, we drew the wave function image at energy level $E = 0.74\ eV$ in Fig. 8(a.3). The overlap of wave functions of the PEDOT:PSS and the Si substrate denotes that the electron transmission from the PEDOT:PSS into the silicon should also be adiabatic. However, the wave function images on the two PEDOT chains do not overlap, which denotes the electron transmission in the stacking direction of PEDOT chains should be nonadiabatic. Therefore, the electron transmission in the PEDOT:PSS membrane is anisotropy.

No matter in the maps for hole and electron, there is no wave function distributed on the Tos group. This phenomenon indicates that the Tos will not participate in the carrier transmission, which is consistent with the fact that the conductivity of a PEDOT:PSS membrane can be improved by reducing the proportion of PSS [39].

Fig. 8(b) and (c) are the DOS diagrams of the Si/PEDOT:PSS systems with methyl and silicon oxide passivation layers, respectively. We can obtain the following conclusions using the analytical method similar to the above (detailed analysis process in Supplementary Material S5). The hole transmission through the Si/PEDOT:PSS interface is nonadiabatic

in both passivation cases, but it can transmit adiabatic between PEDOT layers (as demonstrated in ref 41). The electron transmission from the PEDOT:PSS layer to the Si substrate is adiabatic in both passivation cases, but its transmission in the stacking direction of PEDOT is nonadiabatic.

3.4. Carrier transmission rate through the interface

Quantitative comparison of the effect of the two passivation methods on the carrier transmission through the interface requires the calculation of the orbit coupling coefficient, which is defined as the spatial integral of the product of two orbital wave functions,

$$s_{ij} = \int d^3 r \left| \Psi_i(r) \right| \left| \Psi_j(r) \right| \tag{1}$$

where S_{ij} denotes the coupling coefficient between orbital i and j, Ψ is the wave function. It can quantitatively represent the rate of carrier transport between the two orbits. At the Si/PEDOT:PSS interface, there will be two carrier transport processes: the extraction of holes from orbital Si-VBM to PEDOT:PSS-HOMO and the injection of electrons from orbital PEDOT:PSS-HOMO to Si-CBM. Therefore, the carrier transmission rate through the interface can be reflected by S_{ij} between Si-VBM and PEDOT:PSS-HOMO and between Si-CBM and PEDOT:PSS-HOMO. It should be noted that in the bare Si/PEDOT:PSS system, the wave

functions of Si and PEDOT:PSS can't be distinguished. Therefore, only S_{ij} for the passivated systems was given in Table 2.

For the extraction of holes at the interface, the value of S_{ij} between PEDOT:PSS-HOMO and Si-VBM for the methyl passivated system, 0.036, is significantly greater than that for the silicon oxide passivated system, 0.002. Therefore, methyl passivation is better than silicon oxide passivation for separating holes at the Si/PEDOT:PSS interface.

The value of S_{ij} between PEDOT:PSS-HOMO and Si-CBM for the methyl passivated system, 0.086, is also significantly greater than that for the silicon oxide passivated system, 0.003. Therefore, methyl passivation is also better than silicon oxide passivation for separating electrons.

3.5. Additional electric field through the interface

Charge transfer through the interface can bring an additional electric field, promoting or hindering the separation of carriers at the interface. To this end, we have counted the Mulliken charge populations of each sublayer (the Si substrate, the passivation layer, and the PEDOT:PSS layer), as shown in Table 3. A negative value means electrons enrichment, and a positive value means electrons lost. The results are also plotted in a schematic diagram, Fig. 9, to illustrate the charge transfer.

Fig. 9 shows that for the bare Si/PEDOT:PSS system, a first increasing then decreasing electrostatic potential from the Si substrate to the PEDOT:PSS layer will be generated. This electrostatic potential will bring an energy barrier for the transport of holes and electrons.

In the methyl passivated Si/PEDOT:PSS system, 2.45 e will be transferred from the Si substrate, of which 2.28 e will be captured by the methyl layer and 0.17 e will be transferred to the PEDOT:PSS layer. As a result, a monotonously decreasing electrostatic potential will be formed from the Si substrate to the PEDOT:PSS layer. This electrostatic potential can provide a driving force for the cross-interface transmission of both the electrons and holes.

For the silicon oxide passivated Si/PEDOT:PSS interface, an gradually increasing electrostatic potential from Si to PEDOT:PSS will be generated. Such an electrostatic potential will bring an obstacle to the cross-interface transmission of both the holes and electrons carrier.

To describe the influence of charge transfer on the carrier cross-interface transmission quantitatively, we have also calculated the interface dipole moment μ.

$$\mu = A \int_{a/2}^{a+h/2} z\Delta\rho(z)dz \tag{2}$$

where A denotes the area of the Si/PEDOT:PSS interface, a is the thickness of the Si substrate, and h is thickness of the vacuum layer. The results in Table 3 show that only the interface dipole moment in the methyl passivated system is positive, providing a boost for carriers' transmission across the interface. It should be noted that, limited by the size of the model can be used in the first-principle calculations, the thickness of the Si substrate and PEDOT:PSS is too small relative to the actual interface. Consequently, the passivation layer appears to be extra thick, especially for the silicon oxide passivation layer. Therefore, the results of the cross-interface charge transmission and interface dipole moment have only relative significance.

Therefore, methyl passivation is also better than silicon oxide passivation from the perspective of the charge transfer through the

Table 2
S_{ij} at the methyl and silicon oxide passivated Si/PEDOT:PSS interfaces.

Systems	Ψ_1	Ψ_2	S_{ij}
methyl passivated Si	*PEDOT-HOMO*	*Si-VBM*	0.036
		Si-CBM	0.086
silicon oxide passivated Si	*PEDOT-HOMO*	*Si-VBM*	0.002
		Si-CBM	0.003

Table 3
Mulliken charge population and interface dipole moment μ.

Systems	Si (e)	passivation layer (e)	PEDOT: PSS (e)	μ (e·Å)
bare Si	−0.22	0.24	−0.02	−0.38
CH$_3$- Si	2.45	−2.28	−0.17	0.91
SiO$_x$- Si	−1.22	1.18	0.04	−0.48

interface.

3.6. Bands matching at the interface

PEDOT:PSS is a conductor; therefore, its Fermi energy level should locate at the measured HOMO energy level, 5.0 eV. Assuming that the Si substrate is infinitely thick, the Si-VBM and the Si-CBM's energy levels should equal those of bulk silicon, 5.17 eV and 4.05 eV, respectively. After forming Si/PEDOT:PSS heterojunction, the energy band on the silicon side will bend, with the degree that can be determined by analyzing the DOS diagram.

In Fig. 10a, the position of the Fermi level of the PEDOT:PSS layer is determined by comparing its PDOS curve with that of the PEDOT:PSS crystal in Fig. S3c. It is denoted by a red dotted line located at about 0.25 eV. The VBM of Si is determined by comparing its PDOS with that of the bare Si substrate in Fig. 7a. A blue dotted line at about −0.1 eV denotes it. These two energy levels mark the relative positions of the PEDOT: PSS-HOMO and Si-VBM; therefore, we can evaluate the Si-VBM to be $5.0 + (0.25 + 0.1) = 5.35$ eV at the interface, as illustrated in Fig. 10d. The energy band of Si bends downward by only 0.18 eV at the interface, which will not significantly affect the cross-interface transmission of holes.

The energy band matching at the interface for the methyl and silicon oxide passivated systems are shown in Fig. 10e and f, respectively. In the methyl passivated Si/PEDOT:PSS system, the energy band of Si bends downward by ∼ 0.08 eV at the interface, which is even smaller than that in the bare Si/PEDOT:PSS system. However, in the silicon oxide passivated system, the energy band of Si bends downward by ∼ 0.63 eV, which will hinder the transmission of holes through the interface significantly. The holes need to be tunneled through this barrier; therefore, it is crucial to control the thickness of the silicon oxide layer in fabricating the Si/PEDOT:PSS solar cells.

Comprehensively, the methyl passivation should also be better than silicon oxide passivation from the aspect of band matching at the Si/PEDOT:PSS interface. Here, the band bending situations are not wholly consistent with those reported in ref.18. These differences can be attributed to the limited size of our model, especially in the case of silicon oxide passivation. However, in the first-principle calculations, the obtained energy levels not only contain the influence of the built-in electric field. The complex chemical environment and stress at the interface will also bring impact on the energy levels near the Fermi energy level. Therefore, the band bending results here can complement the experimental data to help us understand the effect of passivation more accurately.

3.7. Comparison of the two passivation methods

Table 4 lists the defect levels, effective carrier mass, carrier transmission type, carrier transmission driving force, orbital coupling coefficient, and band matching for the Si/PEDOT:PSS interface. It can be concluded that both methyl and silicon oxide can efficiently passivate the Si substrate; while, methyl passivation is better than silicon oxide passivation from every aspect.

4. Conclusions

Based on first-principles calculations, we investigated the reasons why methyl passivation is superior to silicon oxide passivation for Si/
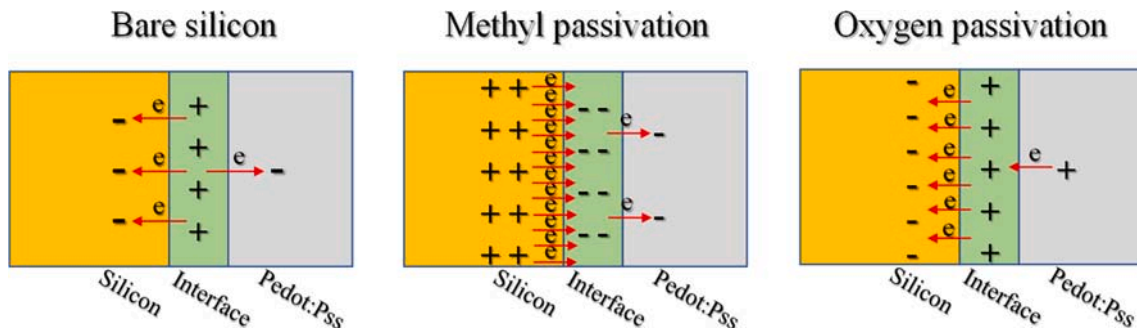
Fig. 9. Schematic diagram of charge transfer through the interface.
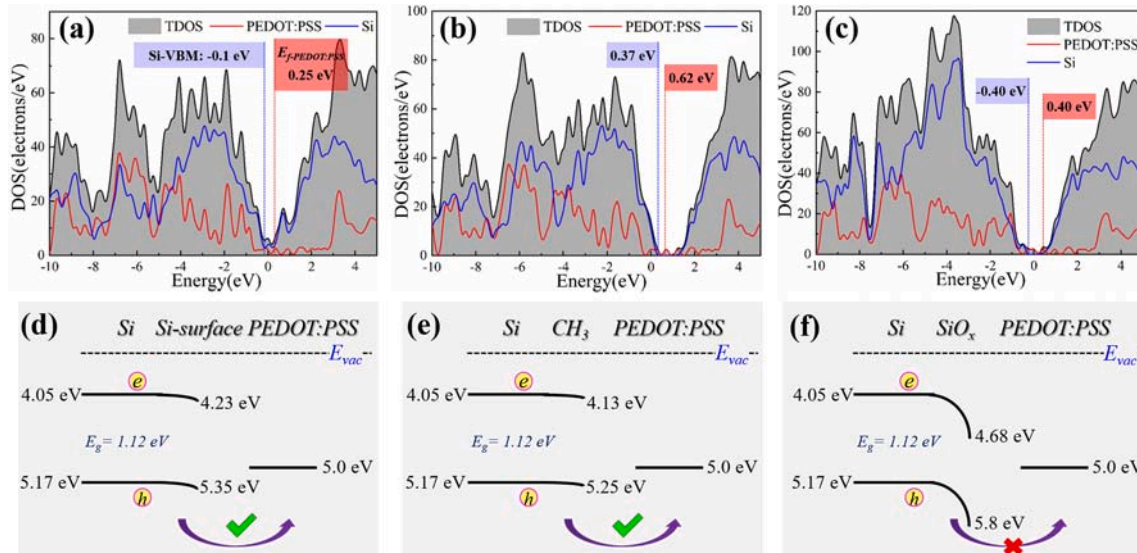

Fig. 10. DOS diagrams of the (a) bare, (b) methyl passivated, and (c) silicon oxide passivated Si/PEDOT:PSS systems; energy band matching of the (d) bare, (e) methyl passivated, and (f) silicon oxide passivated systems.

Table 4
Carrier transmission behaviors through the Si/PEDOT:PSS interface.

Systems		bare Si	CH₃—Si	SiOₓ—Si
defect levels		many, deep	/	few, shallow
effective mass	hole	$-5.58\,m_0$	$-0.33\,m_0$	$-3.73\,m_0$
	electron	$0.74\,m_0$	$0.45\,m_0$	$0.38\,m_0$
transmission type	hole	adiabatic	non-adiabatic	non-adiabatic
	electron	adiabatic	adiabatic	adiabatic
orbital coupling coefficient	hole	/	~0.036	~0.002
	electron	/	~0.086	~0.003
transmission driving force	hole	hindrance	boost	hindrance
	electron	hindrance	boost	hindrance
band matching	hole	slight hindrance	slight hindrance	strong hindrance

PEDOT:PSS solar cells. The results show that both methyl and silicon oxide can efficiently reduce the defect states on the Si substrate. However, methyl passivation is better than silicon oxide passivation in many aspects.

The methyl can eliminate the defect states on the Si substrate more thoroughly than the silicon oxide layer. It can reduce the effective carrier mass in the Si substrate more significantly. In the methyl passivation case, the orbital coupling coefficients between Si-VBM and PEDOT-HOMO, and between Si-CBM and PEDOT-HOMO are an order of magnitude larger than those in the silicon oxide passivation system. In the methyl passivation case, a positive dipole moment of 0.91 e·Å can be formed, which can boost the separation of the carrier at the interface; while in the silicon oxide passivation case, a negative dipole moment of 0.48 e·Å will be formed, which tend to hinder the carrier separation. At the methyl passivated interface, the energy band of silicon bends downward by only ∼ 0.08 eV. At the same time, the value is ∼ 0.63 eV at the silicon oxide passivated Si/PEDOT:PSS interface, which may hinder the hole extraction significantly. This study provides a strategy for evaluating various passivation methods based on first-principle calculations.

Fundings

CRediT authorship contribution statement

Yingfeng Li: Conceptualization, Methodology, Validation, Writing – review & editing, Project administration. **Bingxin Wang:** Resources,

Software, Writing – original draft. **Mengqi Cui:** Investigation, Formal analysis. **Xiang Li:** Data curation, Visualization. **Meicheng Li:** Supervision, Funding acquisition.

Declaration of Competing Interest

The authors declare that they have no known competing financial interests or personal relationships that could have appeared to influence the work reported in this paper.

Appendix A. Supplementary material

Supplementary data to this article can be found online at https://doi.org/10.1016/j.apsusc.2022.153710.

References

[1] M.A. Green, Y. Hishikawa, W. Warta, E.D. Dunlop, D.H. Levi, J. Hohl-Ebinger, A.W. H. Ho-Baillie, Sol. Cell Efficiency Tables. Prog. Photovolt. 25 (2017) 668–676.

[2] Q. Fan, W. Su, Y. Wang, B. Guo, Y. Jiang, X. Guo, F. Liu, T.P. Russell, M. Zhang, Y. Li, Synergistic effect of fluorination on both donor and acceptor materials for high performance non-fullerene polymer solar cells with 13.5% efficiency, Sci. China Chem. 61 (2018) 531–537.

[3] Q. Fan, Y. Wang, M. Zhang, B. Wu, X. Guo, Y. Jiang, W. Li, B. Guo, C. Ye, W. Su, J. Fang, X. Ou, F. Liu, Z. Wei, T.C. Sum, T.P. Russell, Y. Li, High-performance As-Cast nonfullerene polymer solar cells with thicker active layer and large area exceeding 11% power conversion efficiency, Adv. Mater. 30 (2018) 1704546.

[4] Z. Luo, H. Bin, T. Liu, Z.G. Zhang, Y. Yang, C. Zhong, B. Qiu, G. Li, W. Gao, D. Xie, K. Wu, Y. Sun, F. Liu, Y. Li, C. Yang, Fine-tuning of molecular packing and energy level through methyl substitution enabling excellent small molecule acceptors for nonfullerene polymer solar cells with efficiency up to 12.54%, Adv. Mater. 30 (2018) 1706124.

[5] J. He, P. Gao, Z. Yang, J. Yu, W. Yu, Y. Zhang, J. Sheng, J. Ye, J.C. Amine, Y. Cui, Silicon/Organic hybrid solar cells with 16.2% efficiency and improved stability by formation of conformal heterojunction coating and moisture-resistant capping layer, Adv. Mater. 29 (2017) 1606321.

[6] T. Subramani, J. Chen, Y.-L. Sun, W. Jevasuwan, N. Fukata, High-efficiency silicon hybrid solar cells employing nanocrystalline Si quantum dots and Si nanotips for energy management, Nano Energy 35 (2017) 154–160.

[7] S.-S. Yoon, D.-Y. Khang, High efficiency (> 17%) Si-organic hybrid solar cells by simultaneous structural, electrical, and interfacial engineering via low-temperature processes, Adv. Energy Mater. 8 (2018) 1702655.

[8] S. Zhang, Y. Qin, J. Zhu, J. Hou, Over 14% efficiency in polymer solar cells enabled by a chlorinated polymer donor, Adv. Mater. 30 (2018) 1800868.

[9] L. He, Rusli, C. Jiang, H. Wang, D. Lai, Simple approach of fabricating high efficiency si nanowire/conductive polymer hybrid solar cells, IEEE Electron. Device Lett. 32 (2011) 1406–1408.

[10] L. He, D. Lai, H. Wang, C. Jiang, Rusli, High-efficiency si/polymer hybrid solar cells based on synergistic surface texturing of Si nanowires on pyramids, Small 8 (2012) 1664–1668.

[11] D. Liu, Y. Zhang, X. Fang, F. Zhang, T. Song, B. Sun, An 11%-Power-conversion-efficiency organic-inorganic hybrid solar cell achieved by facile organic passivation, IEEE Electron Device Lett. 34 (2013) 345–347.

[12] W. Lu, C. Wang, W. Yue, L. Chen, Si/PEDOT:PSS core/shell nanowire arrays for efficient hybrid solar cells, Nanoscale 3 (2011) 3631–3634.

[13] F. Zhang, D. Liu, Y. Zhang, H. Wei, T. Song, B. Sun, Methyl/allyl monolayer on silicon: efficient surface passivation for silicon-conjugated polymer hybrid solar cell, ACS Appl. Mater. Interfaces 5 (2013) 4678–4684.

[14] R.E. Schlier, H.E. Farnsworth, Structure and adsorption characteristics of clean surfaces of germanium and silicon, J. Phys. Chem. 32 (1959) 917–926.

[15] R. Liu, S.T. Lee, B. Sun, 13.8% Efficiency hybrid Si/organic heterojunction solar cells with MoO₃ film as antireflection and inversion induced layer, Adv. Mater. 26 (2014) 6007–6012.

[16] X. Shen, B. Sun, D. Liu, S.T. Lee, Hybrid heterojunction solar cell based on organic-inorganic silicon nanowire array architecture, J. Am. Chem. Soc. 133 (2011) 19408–19415.

[17] H.-J. Syu, S.-C. Shiu, C.-F. Lin, Silicon nanowire/organic hybrid solar cell with efficiency of 8.40%. Sol. Energy Mater Sol. Cells. 98 (2012) 267-272.

[18] F. Zhang, B. Sun, T. Song, X. Zhu, S. Lee, Air Stable, Efficient Hybrid Photovoltaic Devices Based on Poly(3-hexylthiophene) and Silicon Nanostructures, Chem. Mater. 23 (2011) 2084–2090.

[19] Y. Li, P. Fu, R. Li, M. Li, Y. Luo, D. Song, Ultrathin flexible planar crystalline-silicon/polymer hybrid solar cell with 5.68% efficiency by effective passivation, Appl. Surf. Sci. 366 (2016) 494–498.

[20] P. Cui, D. Wei, J. Ji, H. Huang, E. Jia, S. Dou, T. Wang, W. Wang, M. Li, Planar p–n homojunction perovskite solar cells with efficiency exceeding 21.3%, Nat. Energy 4 (2019) 150–159.

[21] K.H. Hong, J. Kim, J.H. Lee, J. Shin, U.I. Chung, Asymmetric doping in silicon nanostructures: the impact of surface dangling bonds, Nano Lett. 10 (2010) 1671–1676.

[22] H. Peelaers, B. Partoens, F.M. Peeters, First-principles study of doped Si and Ge nanowires, Physica E Low Dimens. Syst. Nanostruct. 40 (6) (2008) 2169–2171.

[23] Y.-J. Ko, M. Shin, S. Lee, K.W. Park, Effects of atomistic defects on coherent electron transmission in Si nanowires: Full band calculations, J. Appl. Phys. 89 (2001) 374–379.

[24] A. Ourmazd, D.W. Taylor, J.A. Rentschler, J. Bevk, Si→SiO₂ transformation: Interfacial structure and mechanism, Phys. Rev. Lett. 59 (1987) 213–216.

[25] A. Calborean, L. Buimaga-Iarinca, F. Graur, DFT charge transfer of hybrid molecular ferrocene/Si structures, Phys. Scr. 90 (2015) 055803.

[26] S.A. Saraireh, S.R. Schofield, P.V. Smith, M.W. Radny, B.V. King, Towards hybrid silicon-organic molecular electronics: The stability of acetone on the Si(001) surface, Surf. Sci. 601 (24) (2007) 5757–5761.

[27] M. Dürr, U. Höfer, Hydrogen diffusion on silicon surfaces, Prog. Surf. Sci. 88 (2013) 61–101.

[28] R.L. Smith, D.R. Bowler, Alane adsorption and dissociation on the Si(0 0 1) surface, J. Phys.: Condens. Matter 29 (2017), 395001.

[29] N. Takeuchi, Y. Kanai, Cooperative Chiral Adsorption of Styrene Molecules on the Si(001)-c(2 × 4) Surface: First-Principles Investigation of Reaction Mechanisms, J. Phys. Chem. C 115 (2011) 14213–14218.

[30] C.G. Wang, K. Huang, W. Ji, Dissociative adsorption of CH(3)X (X = Br and Cl) on a silicon(100) surface revisited by density functional theory, J. Chem. Phys. 141 (2014), 174701.

[31] Y.T. Lee, J.S. Lin, Ab initio molecular dynamics study of ethylene adsorption onto Si(001) surface: short-time Fourier transform analysis of structural coordinate autocorrelation function, J. Comput. Chem. 34 (2013) 2697–2706.

[32] M.V. Fernandez-Serra, C. Adessi, X. Blase, Conductance, surface traps, and passivation in doped silicon nanowires, Nano Lett. 6 (2006) 2674–2678.

[33] A. Pasquarello, M.S. Hybertsen, R. Car, Theory of Si 2p core-level shifts at the Si (001)-SiO2 Interface, Phys. Rev. B: Condens. Matter 53 (1996) 10942–10950.

[34] L. Ley, S. Kowalczyk, R. Pollak, D.A. Shirley, X-Ray photoemission spectra of crystalline and amorphous Si and Ge valence bands, Phys. Rev. Lett. 29 (1972) 1088–1092.

[35] A. Pasquarello, M.S. Hybertsen, R. Car, Si 2p core-level shifts at the Si(001)-SiO₂ Interface: a first-principles study, Phys. Rev. Lett. 74 (1995) 1024–1027.

[36] Y. Cai, Y. Guo, X. Xu, B. Jiang, First-principle investigation 3,4-ethylenedioxy-thiophene molecule adsorption on Cu(110)-(2 × 1)O surface, Surf. Sci. 665 (2017) 83–88.

[37] A.M. Nardes, R.A.J. Janssen, M. Kemerink, A morphological model for the solvent-enhanced conductivity of PEDOT:PSS thin films, Adv. Funct. Mater. 18 (6) (2008) 865–871.

[38] E.G. Kim, J.L. Bredas, Electronic evolution of poly(3,4-ethylenedioxythiophene) (PEDOT): from the isolated chain to the pristine and heavily doped crystals, J. Am. Chem. Soc. 130 (2008) 16880–16889.

[39] A. de Izarra, S. Park, J. Lee, Y. Lansac, Y.H. Jang, Ionic Liquid designed for PEDOT: PSS conductivity enhancement, J. Am. Chem. Soc. 140 (16) (2018) 5375–5384.

[40] R.-Q. Png, P.-J. Chia, S. Sivaramakrishnan, L.-Y. Wong, M. Zhou, L.-L. Chua, P.K. H. Ho, Electromigration of the conducting polymer in organic semiconductor devices and its stabilization by cross-linking, Appl. Phys. Lett. 91 (2007), 013511.

[41] M. Matsui, M. Akaogi, Molecular dynamics simulation of the structural and physical properties of the four polymorphs of TiO₂, Mol. Simulat. 6 (1991) 239–244.

[42] H. Guo, X. Qiu, J. Zhou, Self-assembled core-shell and Janus microphase separated structures of polymer blends in aqueous solution, J. Chem. Phys. 139 (2013), 084907.

[43] T. Yan, Y. Wang, C. Knox, On the structure of ionic liquids: comparisons between electronically polarizable and nonpolarizable models I, J. Phys. Chem. B 114 (2010) 6905–6921.

[44] A. Bansal, H. Mishra, S. Bhattacharya, B.R. Singh, First principles calculations of bonding and charges at the Al₂ interface in a c-Si/SiO₂O₃ interface in a c-Si/SiO₂/am-Al₂O₃ structure applicable for the surface passivation of silicon-based solar cells, IEEE Trans. Electron Devices 63 (2016) 544–550.

[45] P.-X. Lu, L.-B. Qu, Q.-H. Cheng, A comparison study on the electronic structures, lattice dynamics and thermoelectric properties of bulk silicon and silicon nanotubes, Chinese Phys. B. 22 (2013), 117101.